Kinetic Study of the $C_{10}H_7 + O_2$ Reaction

J. Park,* Z. F. Xu, and M. C. Lin*

Department of Chemistry, Emory University, 1515 Dickey Drive, Atlanta, Georgia 30322

Received: January 21, 2009; Revised Manuscript Received: March 6, 2009

The effect of temperature on the formation of $C_{10}H_7O_2$ in the $C_{10}H_7 + O_2$ reaction has been investigated at temperatures 299−444 K by directly monitoring the $C_{10}H_7O_2$ radical in the visible region by cavity ringdown spectrometry (CRDS) using the 2-$C_{10}H_7$Br as a radical source photolyzing at 193 nm. The first experimentally measured rate constant for the association reaction can be given by $k_1 = (1.53 \pm 0.10) \times 10^{12} \exp[(900 \pm 45)/RT]$ cm^3 mol^{-1} s^{-1}, where R is gas constant and 1.986 cal/mol-K, at a total pressure of 40 Torr in the temperature range studied. Theoretically the association process was computed by B3LYP/6-31+G(d, p) with the energy profile improved at the G2MS level of theory. The excitation energies and oscillator strengths of the association product (2-$C_{10}H_7OO$) were calculated by using the time-dependent DFT method. The association rate constant of this reaction was predicted by the canonical VTST/RRKM theory with the steady-state and master-equation analyses. The latter method gave a much better agreement with the experimental data.

1. Introduction

Better understanding of the mechanisms responsible for the formation of polycyclic aromatic hydrocarbons (PAHs), ultimately, to soot, has been one of the most important and challenging problems in hydrocarbon combustion. As small aromatic radicals such as phenyl (C_6H_5), phenylvinyl ($C_6H_5C_2H_2$), naphthyl ($C_{10}H_7$), and their derivatives are believed to play a pivotal role in the formation of naphthalene ($C_{10}H_8$) by HACA (hydrogen-abstraction−acetylene-addition) reactions and cyclization reactions. For example, phenylvinyl radical, which can be formed by the reaction of phenyl radical with acetylene, is believed to be a key intermediate responsible for the formation of naphthalene by its addition to another C_2H_2 molecule.[1] Therefore, naphthyl radicals (see below) play a very significant role in the formation of larger PAHs during the incipient soot formation stages.[2,3]

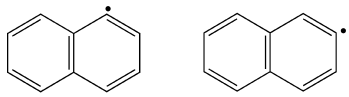

1-$C_{10}H_7$ 2-$C_{10}H_7$

In a kinetic modeling of soot-formation, Green, Howard, and co-workers[3] computed the rate constant for 1-naphthyl reaction with C_2H_2 using TST and QRRK based on the transition-state parameters obtained by B3LYP/cc-pVDZ calculations. Marinov et al.[4] estimated the rate constant of 1-$C_{10}H_7 + O_2$ producing $C_{10}H_7O + O$ in their kinetic modeling of a laminar premixed n-butane flame to be 1×10^{13} cm^3/mol-s. In 2002, Kunioshi[5] and his co-workers calculated the reaction rate of the direct O abstraction reaction, 1-$C_{10}H_7 + O_2 \rightarrow C_{10}H_7O + O$, with a hybrid DFT method at the B3LYP/6-31G(d) level. The $C_{10}H_7 + O_2$ reaction at $T \geq 1000$ K is believed to occur primarily via the metathetical process leading to the formation of a naphthyloxy radical which then can fragment yielding the $C_9H_7 + CO$ products. Similar to the reactions of $C_6H_5 + O_2$ and $C_6H_5C_2H_2 + O_2$, the $C_{10}H_7 + O_2$ reaction at low temperature has been shown to proceed by the association−stabilization process giving rise to the naphthylperoxy radical, $C_{10}H_7 + O_2 \rightarrow C_{10}H_7OO$. To our knowledge, there are no experimental kinetic data on the reaction available in the literature.

In this study we investigated the effect of temperature on the formation of $C_{10}H_7O_2$ in the 2-$C_{10}H_7 + O_2$ reaction at temperatures from 299 to 444 K by directly monitoring the $C_{10}H_7O_2$ radical in the visible region with cavity ringdown spectrometry (CRDS), as have been demonstrated successfully in our previous kinetic measurements of the $C_6H_5 + O_2$ and $C_6H_5C_2H_2 + O_2$ reactions,[6,7] using the 2-$C_{10}H_7$Br as a radical source by photolysis at 193 nm. In addition, the observed kinetic data and associated mechanism have been interpreted with quantum-chemical calculations using quantum chemical density functional theory (DFT) and time-dependent density functional theory (TD-DFT). Since most experimental measurements are limited to low temperature (<1000 K) and pressure (<1 atm), these data may not be directly applied to typical combustion conditions where soot formation is important at higher temperature and pressure (in which the reaction mechanism also changes dramatically and is typically very complex). Therefore, the combination of experimental and theoretical studies should be crucial to our understanding of the mechanism and prediction of the associated rate constant in the much higher temperature and pressure regimes.

2. Experimental Methodologies

CRDS. The CRDS technique was employed for the kinetic study of $C_{10}H_7O_2$ radical formation in the $C_{10}H_7 + O_2$ reaction. All experiments were performed under slow-flow conditions using Ar as the carrier gas at the total pressure of 40 Torr. The flow reactor cell of about 500 cm^3 consists of a heatable Pyrex glass tube attached with two pairs of laser windows opposite to each other, permitting the two-split photolysis laser beams to cross at the center of the reactor at a 30° angle. The reactor was vacuum-sealed at the ends with a pair of highly reflective mirrors ($R = 0.9999$ at 500 nm, radius curvature 6 m), which form a high quality optical cavity, approximately 50 cm in length. The quality of the cavity is such that a pulse of probing dye laser operating at 500 nm with fwhm $\simeq$ 10 ns can be

* Corresponding authors.

10.1021/jp9006476 CCC: $40.75
Published on Web 04/09/2009

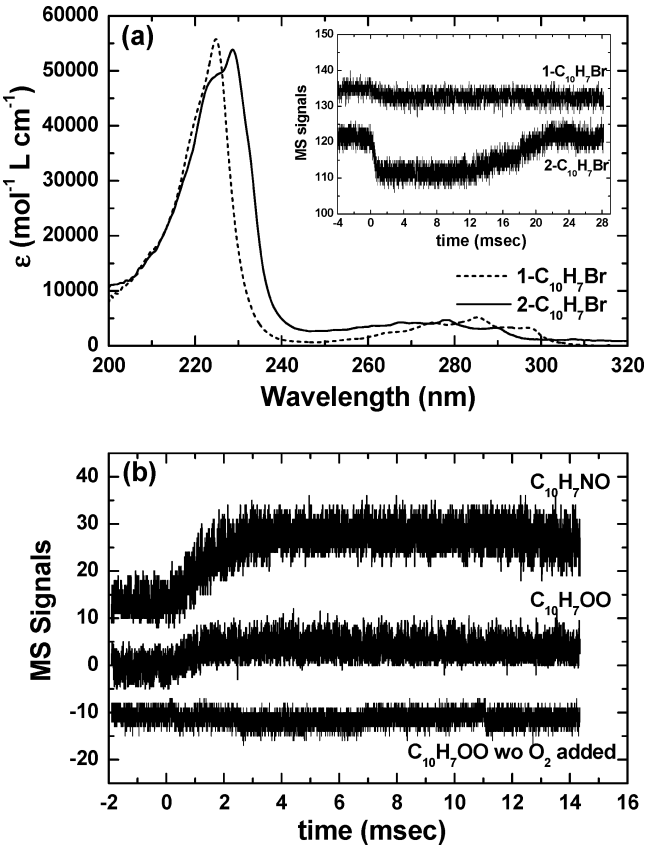

Figure 1. (a) UV absorption spectra of bromonaphthalenes ($C_{10}H_7Br$) in cyclohexane between 200 and 300 nm. Inset: time-resolved PLP/MS signals of bromonaphthalenes ($C_{10}H_7Br$). (b) Typical time-resolved PLP/MS signals of products in the $C_{10}H_7 + O_2$ reaction with and without NO or O_2 added.

lengthened to about 45 μs. The reactor temperature was measured with a calibrated K-type thermocouple (Alumel−Chromel) located below the center of the probe region and maintained within ±0.7 K.

Two pulsed lasers were employed, one for the generation of the $C_{10}H_7$ radical and the other for the detection of $C_{10}H_7O_2$. For radical generation, we employed a Lambda Physik Compex 105 excimer laser at 193 nm (with 2-$C_{10}H_7Br$ as the radical precursor). For the probing of the $C_{10}H_7O_2$ radical, a Lambda Physik excimer laser (EMG201) pumped tunable dye laser (FL3002) was used. It has a half-width of about 10 ns and pulse energy of 1−2 mJ at 500 nm.

The probing laser beam was injected directly into the reactor cavity through one of the mirrors along the axis of the reactor tube. A fraction of the photon pulse transmitted through the second mirror was filtered and detected with a Hamamatsu photomultiplier tube (PMT). Photoelectric signal from the PMT was amplified with a fast preamplifier (SR445) and acquired and averaged with a multichannel digital oscilloscope (LeCroy 140). The averaged signal was stored in a computer for future data analysis. A pulse-delay generator (SR DG 535) interfaced with the computer was employed to control the firing of the two lasers as well as the triggering of the data acquisition system.

The concentration of each individual molecule was obtained by the following formula: $[R] = 9.66 \times 10^{16}$ (%) PF_R/TF_T molecules/cm^3, where % is the percentage of each molecule in its gas mixture, P is the total reaction pressure in Torr, T is the reaction temperature, F_R is the flow rate of each gas mixture, and F_T is the total flow rate of all gases. The typical resident

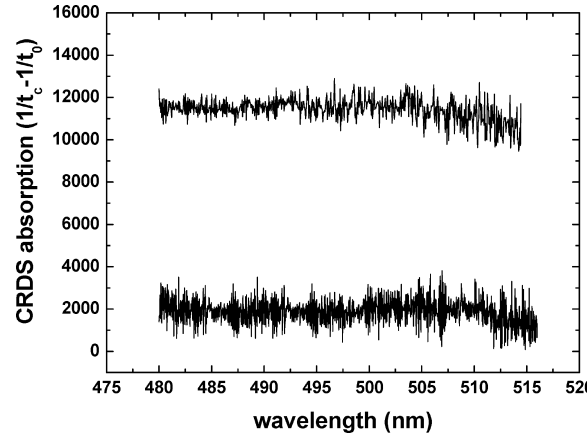

Figure 2. Absorption spectra detected by CRDS at 100 μs after the photolysis of 2-bromonaphthalene at 193 nm in Ar without, (lower trace) and with, (upper trace) added O_2.

time in the probing zone was ∼50 ms, and the repetition rate of 2 Hz allowed enough time for a fresh sample in the reactor between pulses. The effect of slow repetition rate of 1 Hz was negligible in the transient signals. The flow rates were measured by mass flowmeters (MKS, 0258C), and the gas pressure was measured with an MKS Baratron manometer. The initial concentration of 2-$C_{10}H_7Br$ was estimated to be within 0.5−5.0 $\times$ 10^{13} molecules/cm^3.

In kinetic measurements, the CRDS technique was employed to detect the transient concentration of a radical of interest by determining the decay times of the injected probing photons in the absence (t_0) and the presence (t_c) of the radical. The two decay times can be related with the concentration of the absorbing species inside the cavity by eq 1:

$$1/t_c = 1/t_0 + A \exp(-t/\tau) \quad (1)$$

where A is a constant containing the concentration of the absorbing species at time t and experimental parameters such as the cavity length (∼50 cm), the refractive index of the absorbing medium, etc.; τ is the lifetime of the absorbing species inside the cavity.[8]

PLP/MS. The high pressure mass-spectrometric sampling technique (PLP/MS) was employed for the detection of $C_{10}H_7NO$ and $C_{10}H_7OO$ products from the NO and O_2 titration in the photolysis of 2-$C_{10}H_7Br$ at 193 nm. The sampling technique of Saalfeld and co-workers[9,10] has been extensively utilized by Gutman,[11] Koshi, Matsui, and their collaborators[12] for kinetic measurements. The $C_{10}H_7$ radical was generated photolytically with an excimer laser (Lambda Physik COMPex105) in a quartz tubular Saalfeld-type reaction tube which has an inner diameter of 10 mm and a length of 150 mm with a conical sampling hole of 120 μm diameter at the center of the reactor. The reactor was mounted perpendicularly to the detection axis of a quadrupole mass spectrometer (QMS, Extrel model C50) which detects the positive ion signals generated by electron impact (EI).

The detection chamber housing the mass spectrometer was separated from the supersonic expansion chamber which holds the reaction tube by a skimmer (1 mm orifice, Beam Dynamics model 1) mounted at the center of a metal plate. The skimmer was placed 3.0 mm from the sampling hole of the reaction tube. During the experiment, the pressures in the expansion and detection chambers were kept at 5−10 $\times$ 10^{-5} and 5−10 $\times$ 10^{-6} Torr, respectively.

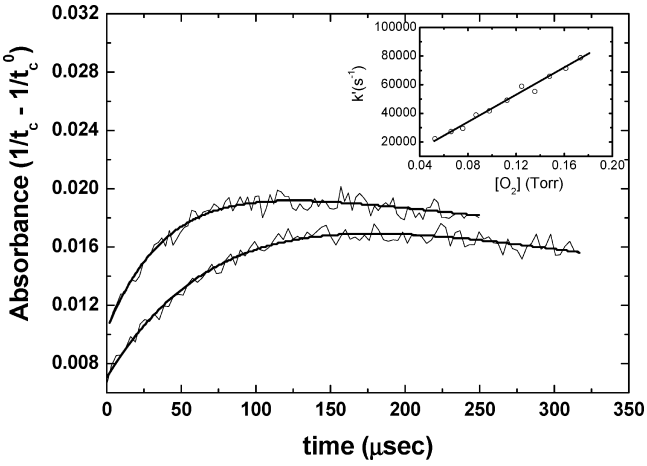

Figure 3. Typical time-resolved absorption plots of $C_{10}H_7O_2$ formed in the $C_{10}H_7 + O_2$ reaction at 298 K with different concentrations of O_2: Top trace: $[O_2] = 0.0957$ Torr; bottom trace: $[O_2] = 0.0297$ Torr, solid curves are fitted values using eq 2. Inset, k' vs $[O_2]$ plot at 298 K.

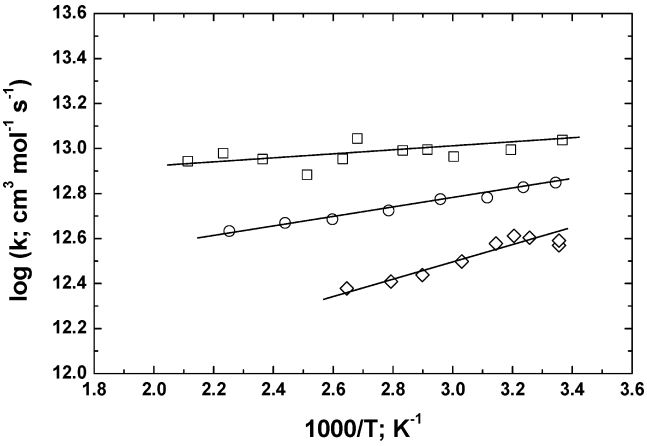

Figure 4. Arrhenius plots for O_2 association reactions with C_6H_5 (□), $C_6H_5C_2H_2$ (◇), and $C_{10}H_7$ (○).

The PLP/MS experiment was carried out under slow-flow conditions with as long as 50 ms resident time, which is considerably longer than most radical reaction times, 1−20 ms. Mixing of reactants and the helium buffer gas was achieved in a stainless bellows tube prior to the introduction into the reaction tube. The concentration of each individual molecule was obtained by the same method as in the CRDS experiment. The mole fraction of 2-$C_{10}H_7Br$ was typically <1.0% and the conversion of 2-$C_{10}H_7Br$ was in the range of 2−5% depending on photolytic laser energy.

2-$C_{10}H_7Br$ (Aldrich, 97%) and NO (Aldrich, 99.5%) were purified by means of the freeze pump-thaw degassing procedure with liquid nitrogen (77 K). He and Ar as a carrier gas and O_2 reactant (Specialty Gases, 99.995% UHP grade) were used without further purification.

3. Results and Discussion

3.1. Experimental Results. The effect of temperature on the formation of $C_{10}H_7O_2$ in the 2-$C_{10}H_7 + O_2$ reaction has been performed at temperatures 299−444 K by directly monitoring the $C_{10}H_7O_2$ radical in the visible region with CRDS using the 2-$C_{10}H_7Br$ as a radical source by photolysis at 193 nm. We selected 2-$C_{10}H_7$ in our study of the naphthyl kinetics because of the stronger extinction coefficient of 2-$C_{10}H_7Br$ than 1-$C_{10}H_7Br$ at 193 nm as confirmed by higher 2-$C_{10}H_7$ yields according to the NO and O_2 titration results in Figure 1a and 1b, respectively, in our PLP/MS measurement.

On the basis of the CRDS spectrum of the phenyl radical first reported by Yu and Lin[8] in the 500−510 nm region, $C_{10}H_7$ may have a detectable absorption in the similar region of the spectrum. To obtain its absorption spectrum, we initially scanned the wavelength from 480 to 520 nm using 0.1% of 2-$C_{10}H_7Br$ diluted in Ar. The result shown in Figure 2 indicates a negligible absorption by the naphthyl radical in the 480−520 nm region. However, the similar scan with a small amount of O_2 revealed a much stronger absorption attributable to $C_{10}H_7O_2$ in the same visible range, similar to the $C_6H_5O_2$, [6] $C_6H_5C_2H_2O_2$,[7] and other cases reported by von Sontag and co-workers.[13]

The typical time-resolved signal of the formation of the $C_{10}H_7O_2$ radical by CRDS is shown in Figure 3. Since the time-resolved signal shows a slow decay which may be due to the diffusion out of the probe beam and/or by secondary radical−radical reactions, the signal was analyzed with the standard consecutive reaction mechanism as:

$$C_{10}H_7 + O_2 \xrightarrow{k_1} C_{10}H_7OO \xrightarrow{k_2} \text{others}$$

using the kinetic equation based on the measured cavity photon decay times t_c and t_0 with and without the radical at time t, respectively:

$$1/t_c - 1/t_0 = B[k_1'/(k_2' - k_1')][\exp(-k_1't) - \exp(-k_2't)] \quad (2)$$

In the above equation, B contains the initial concentration of the radical species of interest and experimental parameters such as the cavity length, etc.[8] Nonlinear fitting of eq 2 to experimental data, as those presented in Figure 3, yields the pseudo-first-order rate coefficients, k_1' for the formation of $C_{10}H_7O_2$ in the presence of a known O_2 concentration. A typical plot of k_1' vs O_2 concentration, as illustrated in the inset of Figure 3, gives the averaged second-order rate constant k_1 from its slope according to the equation, $k_1' = k_0 + k_1[O_2]$, where k_0 is the radical decay constant in the absence of the molecular reactant due to the loss of the radical by diffusion away from the probing beam and/or radical reactions. Both k_0 and k_2 are close to each other and typically in the range of $3-5 \times 10^3$ s^{-1}. A least-squares analysis gives the *first experimentally measured rate constant* for 2-$C_{10}H_7 + O_2$,

$$k_1 = (1.53 \pm 0.10) \times 10^{12} \exp[(900 \pm 45)/RT]\ \text{cm}^3\ \text{mol}^{-1}\ \text{s}^{-1}$$

where R is gas constant and 1.986 cal/mol-K, in the temperature range of 299−444 K at a total pressure of 40 Torr (see Figure 4).

Figure 4 shows the comparison of the kinetic data for the C_6H_5, $C_6H_5C_2H_2$, and $C_{10}H_7$ reactions with O_2. From phenyl to phenylvinyl reactions, the rate constants varied by a factor of 3−5 between 300 and 400 K, and those of the naphthyl reaction lie in-between. To date, although we have established a vast amount of C_6H_5 kinetic data by means of the three complementary kinetic techniques, pulsed laser photolysis/mass spectrometry (PLP/MS),[14] cavity ringdown spectrometer (CRDS),[8] and pyrolysis/FTIR spectrometry (P/FTIRS),[15] there has been no established fact that these kinetic data can be directly transferred to naphthyl and bigger aryl radicals for modeling

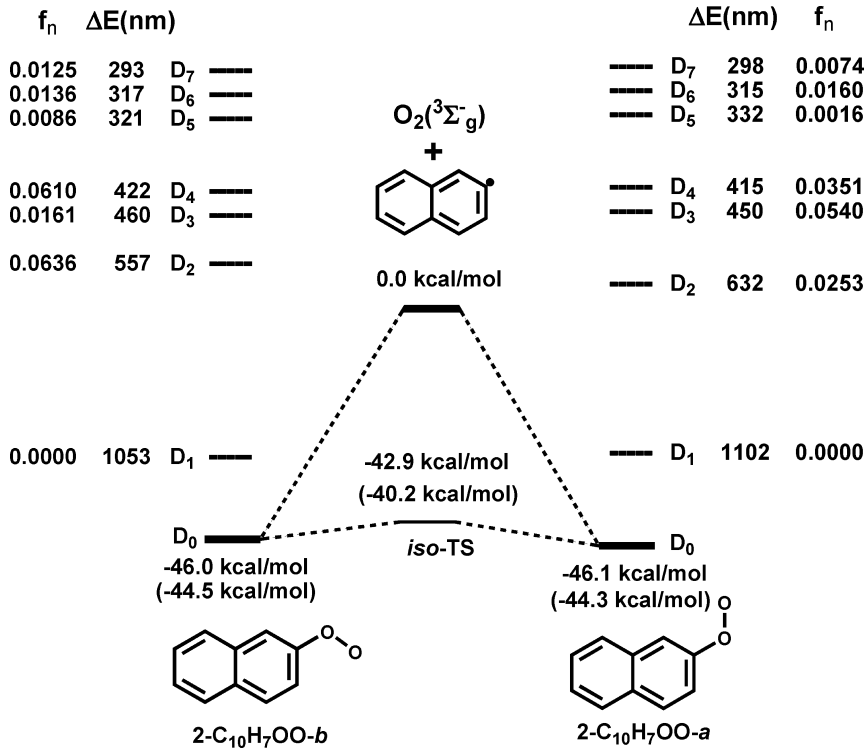

Figure 5. Energetic profile (kcal/mol) of $C_{10}H_7 + O_2(^3\Sigma^-_g)$ calculated at the G2MS/6-31+(d, p) level of theory. Numbers in parentheses were obtained at B3LYP/6-31+(d, p) level. f_n oscillator strength at excitation level D_n and ΔE (nm): absorbing wavelength of excitation.

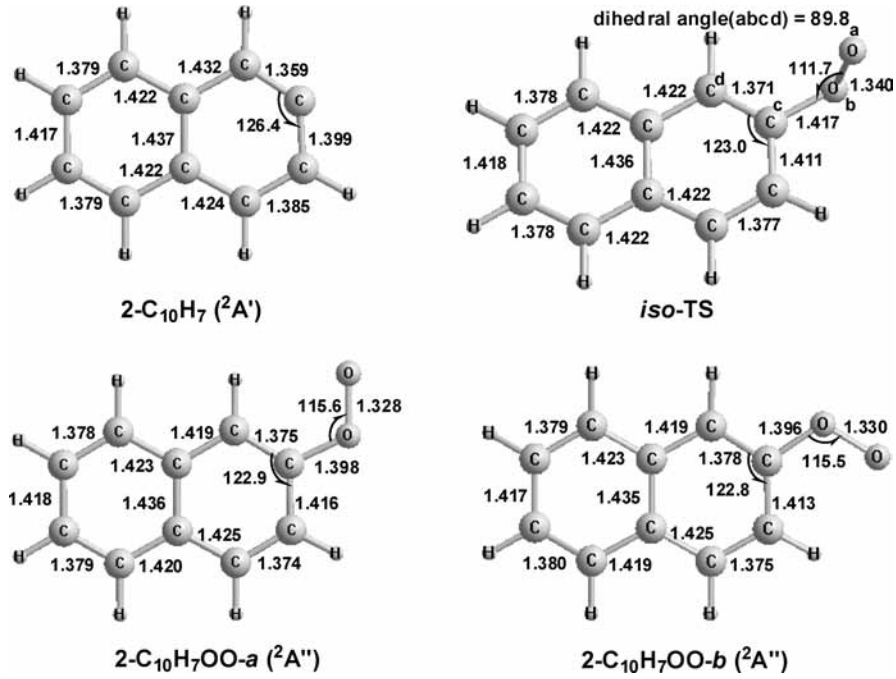

Figure 6. Geometric parameters (bond length in angstroms and angle in degrees) of 2-$C_{10}H_7$, 2-$C_{10}H_7OO$, and iso-TS optimized at the B3LYP/6-31+(d, p) level of theory.

of soot growth. Clearly, there is a need to acquire more kinetic data for bigger aromatic radical reactions beyond phenyl. Additional reliable kinetic data for naphthyl reactions are essential for calibration and establishment of a reliable computational protocol for prediction of larger aryl radical reactions which cannot be readily measured experimentally.

3.2. Theoretical Association Rate. For the association process of the naphthyl radical with the ground-state oxygen molecule, the B3LYP hybrid density functional theory (DFT)[16] with the 6-31+G(d, p) basis set[17] was employed to optimize the geometric parameters of the reactants, association products, and transition state on the doublet state potential energy surface by the Gaussian 03 program.[18] For a more accurate evaluation of the energetic parameters, higher-level single-point energy calculations were carried out by the modified Gaussian-2 (G2MS) method[19] based on the optimized geometries at the B3LYP/6-31+G(d,p) level. Also, the excitation energies and oscillator strengths of 2-$C_{10}H_7OO$ are calculated by using the

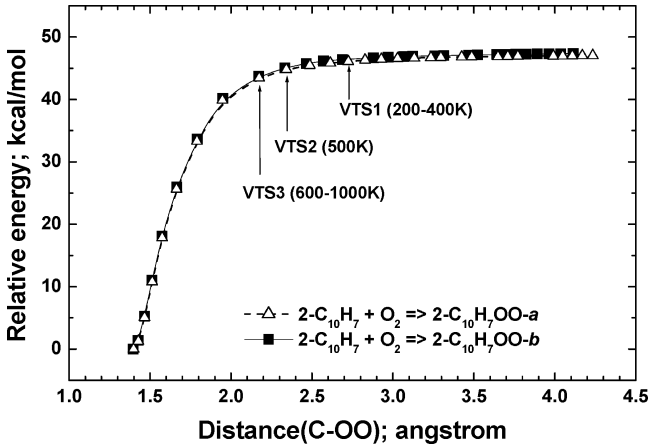

Figure 7. Canonical VTS points at specific temperatures and minimum energy curves versus distance of R(C-OO) in the association process of $C_{10}H_7 + O_2(^3\Sigma^-_g) \rightarrow C_{10}H_7OO$ calculated at the B3LYP/6-31+(d, p) level of theory.

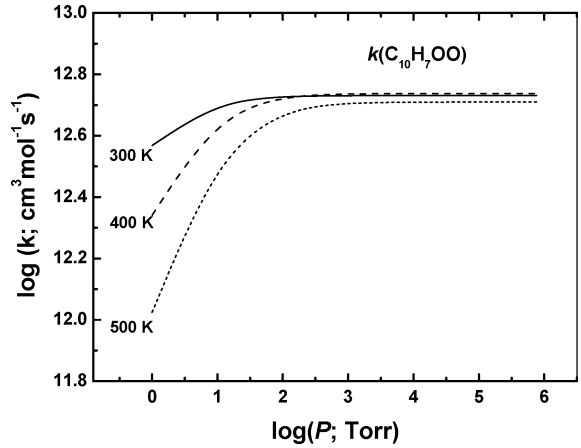

Figure 8. Predicted rate constants for the association reaction of $C_{10}H_7 + O_2(^3\Sigma^-_g)$ versus pressure at 300, 400, and 500 K.

time-dependent DFT method;[20] the result confirms that a strong absorption exists in the visible region of the spectrum (400−600 nm) by both the *a* and *b* conformers of 2-$C_{10}H_7OO$.

Figure 5 displays the energy profile of the 2-$C_{10}H_7 + O_2$ ($^3\Sigma_g$) association reaction and the excitation levels of the association products. The critical geometric parameters of naphthyl, naphthylperoxy, and rotation transition state are shown in Figure 6. The association reaction of 2-$C_{10}H_7 + O_2(^3\Sigma_g)$ is a barrierless process as illustrated in Figure 7 forming the two conformers, 2-$C_{10}H_7OO$-*a* with the terminal oxygen atom inclined toward C1 and 2-$C_{10}H_7OO$-*b* with the terminal oxygen atom inclined toward C3 (see Figures 5 and 6). Both conformers have the state symmetry of $^2A''$. Relative to the $C_{10}H_7 + O_2(^3\Sigma_g)$ reactants, 2-$C_{10}H_7OO$-*a* and 2-$C_{10}H_7OO$-*b* are predicted to be −46.1 and −46.0 kcal/mol, respectively, at the G2MS level, which differ from the values at the B3LYP level less than 1.7 kcal/mol. Because the rotation barrier at iso-TS, in which the terminal oxygen atom rotates around C−O bond axis, is predicted to be only about 3.2 kcal/mol, the isomerization reaction can occur readily and the internal rotation of the -OO group may be considered to be almost free.

Steady-State Rate Calculation. On the basis of the reaction mechanism discussed above, the rate constant measured under the low temperature condition for the association process was predicted with canonical variational TST/RRKM (Rice−Ramsperger−Kassel−Marcus) theory according to the scheme

$$2\text{-}C_{10}H_7 + O_2 \rightleftharpoons 2\text{-}C_{10}H_7OO^* \xrightarrow[[M]]{} 2\text{-}C_{10}H_7OO$$

with the steady-state method.[21,22] On the basis of our previous study of an analogous but smaller $C_6H_5 + O_2$ system under a similar condition, under which the formation of C_6H_5O was directly probed by CRDS but was failed to be detected, the fragmentation of the larger excited 2-naphthylperoxyl radical should be negligible and thus was not considered here.

The rate constant for the collisonal stabilization of the excited adduct, 2-$C_{10}H_7O_2$*, in Ar buffer gas is estimated in the weak-collision approximation according to the relationship by Troe,[23]

$$\frac{\beta_c}{1-\beta_c^{1/2}} = \frac{-\langle \Delta E \rangle_{all}}{F_E k_B T}$$

assuming the average energy transferred in all up and down transitions to be $-\langle \Delta E \rangle_{all} = 1.0$ kcal/mol. β_c is the collisional efficiency, and F_E is the energy dependence factor of the density of states.[23] The Lennard−Jones (*L-J*) parameters of Ar, $\varepsilon/k_B = 114.0$ K and $\sigma = 3.47$ Å, were taken from the literature,[24] while those of 2-$C_{10}H_7O_2$ were approximately taken to be those of naphthalene: $\varepsilon/k_B = 495$ K and $\sigma = 6.44$ Å, computed by its critical temperature (747 K) and critical pressure (40.6 atm).[24,25] The rate constant of the association process was computed by the canonical variational transition state (CVTS) method[21,22,26] based on the criterion of the maximum free energy of activation, $\Delta G^{\ddagger}$, for the barrierless process. Figure 7 shows the CVTS positions at the different temperatures on the minimum energy curves for both 2-$C_{10}H_7 + O_2 \rightarrow$ 2-$C_{10}H_7OO$-*a* and 2-$C_{10}H_7 + O_2 \rightarrow$ 2-$C_{10}H_7OO$-*b*. Both curves are seen to be essentially the same even in the absence of the free torsional motion of the -OO group. The free rotation will make them indistinguishable as one would expect. The harmonic frequencies and moments of inertia of the three canonical variational transition states are listed in Supporting Information for rate constant calculations with the smallest frequencies treated as free internal rotors around the C−O bond with the force constants are 1.824, 1.935, and 2.027 cm^{-1} for VTS1, VTS2, and VTS3, respectively.

The predicted rate constants as a function of pressure at the temperatures of 300, 400, and 500 K are drawn in Figure 8. It can be seen that the pressure-dependent effect of the rate constants of the 2-$C_{10}H_7OO$ formation is positive and this positive dependency diminishes with the pressure increasing until about 100 Torr at 500 K. Above 100 Torr, the rate constant becomes independent of pressure. The predicted temperature effect in 200−1000 K is shown in Figure 9A for comparison of the experimental and theoretical results. Evidently, the rate constants exhibit a small negative temperature dependent at all three pressures of 1, 40, and 760 Torr. In the experimental temperature range of 299−444 K at 40 Torr Ar pressure, the predicted rate constants agree reasonably with the experimental values within the maximum deviation of 24% at 300 K.

Master-Equation Calculation. We have also employed the Variflex code[27] to predict the association rate constant by solving the 1-D master equation (ME) for the association/stabilization process using the same canonical VTST parameters presented in Figure 7 and the collisional quenching parameters employed in the cVTST/RRKM calculations with the steady-state approach. In this calculation, the hindered internal rotations of VTS2 and VTS3 were considered because of the shortened C−O distance. The rotation barrier at VTS2 is estimated to be

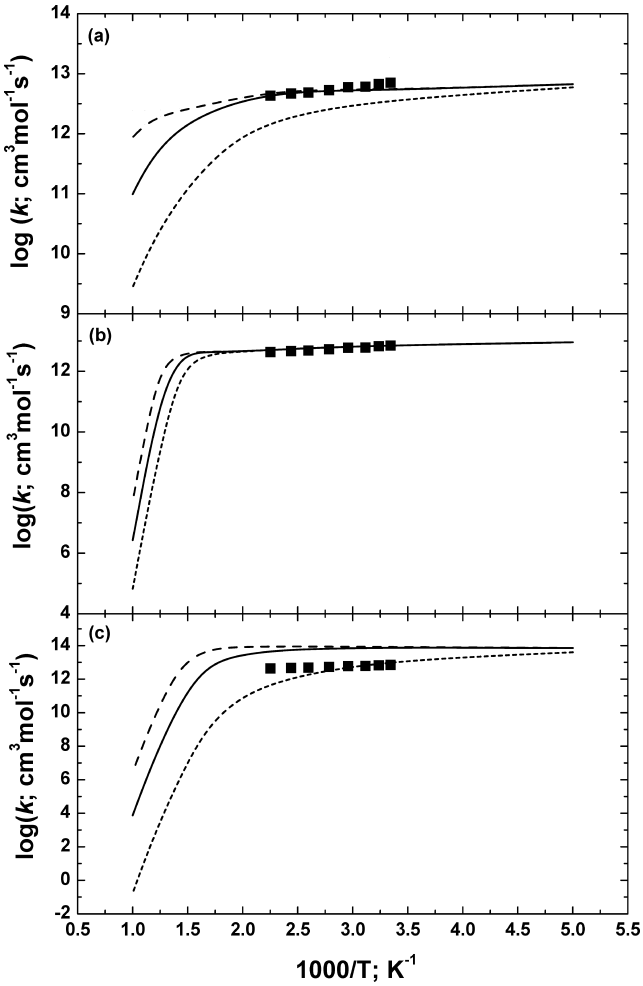

Figure 9. Comparisons of predicted rate constants with experimental data. (a) cVTST/RRKM with steady-state approximation. (b) cVTST/ME calculation. (c) VRC/ME calculation with the Morse function $V(R) = 48.9\{1 - \exp[-4.509(R - 1.370)]\}^2$ kcal/mol. ■, experimental result; dotted curve, 1 Torr; solid curve, 40 Torr; dashed curve, 760 Torr.

495 cm^{-1} at the B3LYP level and that at VTS3 is 829 cm^{-1}. The results of the calculation are presented in Figure 9B. Evidently the agreement between the predicted values and the experimental data is considerably better and has a noticeably weaker pressure-dependence than that predicted by the steady-state approach.

In addition, in order to compare the efficacy of the variable reaction coordinate (VRC) menthod[27,28] with ME analysis for this reaction, the association potential energy, predicted at the B3LYP/6-31+G(d,p) level as in Figure 7 and modeled by the Morse function, $V(R) = 48.9\{1 - \exp[-4.509(R - 1.370)]\}^2$ kcal/mol for the separation $R(C_{10}H_7-O_2) = 1.370$ Å to 4.3 Å, was employed. The VRC/ME result is shown in Figure 9C for different specified pressures. These values appear to be higher than experimental data by about a factor of 10 at the high-pressure limit with the expected much faster falloff in rate constant at lower pressures. The VRC/ME method appears to overestimate the rate constant for this association reaction.

For practical modeling applications in combustion, the predicted rate constants based on canonical VTST/ME calculations are recommended below:

$$k^{\infty} = 4.68 \times 10^{13} T^{-0.396} \exp(96/T) \qquad (200-1000\ \text{K})$$

$$k(760\ \text{Torr Ar}) = 7.99 \times 10^{21} T^{-3.18} \exp(-756/T) \qquad (200-800\ \text{K})$$

$$= 2.59 \times 10^{231} T^{-71.24} \exp(-23000/T) \qquad (800-1000\ \text{K})$$

for the high pressure limit and the atmospheric pressure in units of $cm^3\ mol^{-1}\ s^{-1}$ and

$$k^0 = 4.84 \times 10^{45} T^{-7.84} \exp(-2123/T) \qquad (200-600\ \text{K})$$

$$= 2.14 \times 10^{239} T^{-72.51} \exp(-21426/T) \qquad (600-1000\ \text{K})$$

for the low pressure limit in units of $cm^6\ mol^{-2}\ s^{-1}$.

4. Conclusion

The effect of temperature on the formation of $C_{10}H_7O_2$ in the $C_{10}H_7 + O_2$ reaction has been investigated in the temperature range 299−444 K by directly monitoring the $C_{10}H_7O_2$ radical in the visible region by cavity ringdown spectrometry (CRDS) using the 2-$C_{10}H_7Br$ as a radical source by photolysis at 193 nm. The high pressure mass-spectrometric sampling technique (PLP/MS) was employed to detect $C_{10}H_7NO$ and $C_{10}H_7OO$ products from the NO and O_2 titration in the photolysis of 2-$C_{10}H_7Br$ at 193 nm. The measured rate constant for 2-$C_{10}H_7 + O_2$ can be presented by $k_1 = (1.53 \pm 0.10) \times 10^{12} \exp[(900 \pm 45)/RT]$ $cm^3\ mol^{-1}\ s^{-1}$, where R is gas constant and 1.986 cal/mol-K, in the temperature range of 299−444 K at a total pressure of 40 Torr Ar, effectively reaching its high-pressure limit).

Additionally, the reaction mechanism has been studied at the G2MS//B3LYP/6-31+G(d, p) level. The association process from $C_{10}H_7 + O_2(^3\Sigma_g)$ to 2-$C_{10}H_7OO$ occurs barrierlessly with the exothermicity of 46.1 kcal/mol. The observed spectrum of 2-$C_{10}H_7OO$ at 500 nm was confirmed by its excitation energies and oscillator strengths calculated by the time-dependent DFT method. Theoretically, the best result for the association rate constant of this reaction was obtained by the canonical VTST/ME method, and the predicted value is in good agreement with the experimental data.

Acknowledgment. The authors are grateful for the partial support of this work from the Basic Energy Sciences, Department of Energy, under contract no. DE-FG02-97-ER14784. We also thank the Cherry L. Emerson Center of Emory University for the use of its resources.

Supporting Information Available: The harmonic frequencies and moments of inertia. This information is available free of charge via the Internet at http://pubs.acs.org.

References and Notes

(1) (a) Bockhorn, H.; Fetting, F.; Wenz, H. W. *Ber. Bunsen-Ges. Phys. Chem.* **1983**, *87*, 1067–1073. (b) Frenklach, M.; Clary, D. W.; Gardiner, W. C., Jr.; Stein, S. E. *Proc. Combust. Inst.* **1985**, *20*, 887. (c) Frenklach, M.; Warnatz, J. *Combust. Sci. Technol.* **1987**, *51*, 265–283. (d) Tokmakov, I. V.; Lin, M. C. *J. Am. Chem. Soc.* **2003**, *125*, 11397.

(2) Richter, H.; Benish, T. G.; Mazyar, O. A.; Green, W. H.; Howard, J. B. *Proc. Combust. Inst.* **2008**, *28*, 2609.

(3) Richter, H.; Mazyar, O. A.; Sumathi, R.; Green, W. H.; Howard, J. B.; Bozzelli, J. W. *J. Phys. Chem. A* **2001**, *105*, 1561.

(4) Marinov, N. M.; Pitz, W. J.; Westbrook, C. K.; Vincitore, A. M.; Castaldi, M. J.; Senkan, S. M. *Combust. Flame* **1998**, *114*, 192.

(5) Kunioshi, N.; Touda, M.; Fukutani, S. *Combust. Flame* **2002**, *128*, 292.

(6) Yu, T.; Lin, M. C. *J. Am. Chem. Soc.* **1994**, *116*, 9571–9576.

(7) Park, J.; Lin, M. C. *Proc. Combust. Inst.* **2008**, *32*, 305–310.

(8) (a) Yu, T.; Lin, M. C. *J. Am. Chem. Soc.* **1993**, *115*, 4371. (b) Lin, M. C.; Yu, T. *Int. J. Chem. Kinet.* **1993**, *25*, 875. (c) Park, J.; Lin, M. C. *American Chemical Society Special Publication Series on Cavity Ringdown Spectroscopy*; American Chemical Society: Washington, DC, 1999; Chapter 13, 196.

(9) Wyatt, J. R.; DeCorpo, J. J.; McDowell, M. V.; Saalfeld, F. E. *Rev. Sci. Instrum.* **1974**, *45*, 916.

(10) Wyatt, J. R.; DeCorpo, J. J.; McDowell, M. V.; Saalfeld, F. E. *Int. J. Mass Spectrom. Ion Phys.* **1975**, *16*, 33.

(11) (a) Park, J. Y.; Heaven, M. C.; Gutman, D. *Chem. Phys. Lett.* **1984**, *104*, 469–474. (b) Slagle, I. R.; Park, J. Y.; Heaven, M. C.; Gutman, D. *J. Am. Chem. Soc.* **1984**, *106*, 4356–4361.

(12) Koshi, M.; Miyoshi, A.; Matsui, H. *J. Phys. Chem.* **1991**, *95*, 9869.

(13) Naumov, S.; Clemens, C.; von Sonntag, J. *Phys. Org. Chem.* **2005**, *18* (7), 586–594.

(14) Park, J.; Lin, M. C. *Recent Res. Dev. Phys. Chem.* **1998**, *2*, 965–979.

(15) Park, J.; Dyakov, I. V.; Mebel, A. M.; Lin, M. C. *J. Phys. Chem. A* **1997**, *101*, 6043.

(16) (a) Becke, A. D. *J. Chem. Phys.* **1993**, *98*, 5648. (b) Becke, A. D. *J. Chem. Phys.* **1992**, *96*, 2155. (c) Lee, C.; Yang, W.; Parr, R. G. *Phys. Rev.* **1988**, *37B*, 785.

(17) Pople, J. A.; Head-Gordon, M.; Raghavachari, K. *J. Chem. Phys.* **1987**, *87*, 5968.

(18) Frisch, M. J.; Trucks, G. W.; Schlegel, H. B.; Scuseria, G. E.; Robb, M. A.; Cheeseman, J. R.; Montgomery, J. A., Jr.; Vreven, T.; Kudin, K. N.; Burant, J. C.; Millam, J. M.; Iyengar, S. S.; Tomasi, J.; Barone, V.; Mennucci, B.; Cossi, M.; Scalmani, G.; Rega, N.; Petersson, G. A.; Nakatsuji, H.; Hada, M.; Ehara, M.; Toyota, K.; Fukuda, R.; Hasegawa, J.; Ishida, M.; Nakajima, T.; Honda, Y.; Kitao, O.; Nakai, H.; Klene, M.; Li, X.; Knox, J. E.; Hratchian, H. P.; Cross, J. B.; Bakken, V.; Adamo, C.; Jaramillo, J.; Gomperts, R.; Stratmann, R. E.; Yazyev, O.; Austin, A. J.; Cammi, R.; Pomelli, C.; Ochterski, J. W.; Ayala, P. Y.; Morokuma, K.; Voth, G. A.; Salvador, P.; Dannenberg, J. J.; Zakrzewski, V. G.; Dapprich, S.; Daniels, A. D.; Strain, M. C.; Farkas, O.; Malick, D. K.; Rabuck, A. D.; Raghavachari, K.; Foresman, J. B.; Ortiz, J. V.; Cui, Q.; Baboul, A. G.; Clifford, S.; Cioslowski, J.; Stefanov, B. B.; Liu, G.; Liashenko, A.; Piskorz, P.; Komaromi, I.; Martin, R. L.; Fox, D. J.; Keith, T.; Al-Laham, M. A.; Peng, C. Y.; Nanayakkara, A.; Challacombe, M.; Gill, P. M. W.; Johnson, B.; Chen, W.; Wong, M. W.; Gonzalez, C.; Pople, J. A. *Gaussian 03, Revision B.03*; Gaussian, Inc., Pittsburgh, PA, 2003.

(19) Robert, D. J.; Froese, S. H.; Svensson, M.; Morokuma, K. *J. Phys. Chem. A* **1997**, *101* (2), 227.

(20) Stratmann, E.; Scuseria, G. E.; Frisch, M. J. *J. Chem. Phys.* **1998**, *109*, 8218.

(21) Hsu, C.-C.; Mebel, A. M.; Lin, M. C. *J. Chem. Phys.* **1996**, *105*, 2346.

(22) Chakraborty, D.; Hsu, C.-C.; Lin, M. C. *J. Chem. Phys.* **1998**, *109*, 8889.

(23) Troe, J. *J. Phys. Chem.* **1979**, *83*, 114.

(24) Hippler, H.; Troe, J.; Wendelken, H. J. *J. Chem. Phys.* **1983**, *78*, 6709.

(25) Lide, D. R. *CRC Handbook of Chemistry and Physics*, 71st ed.; CRC Press: Boca Raton, FL, 1990; Vol. 6, p 49.

(26) Garret, B. C.; Truhlar, D. G. *J. Chem. Phys.* **1979**, *70*, 1593.

(27) Klippenstein, S. J.; Wagner, A. F.; Dunbar, R. C.; Wardlaw, D. M.; Robertson, S. H. VARIFLEX: version 1.00, Argonne National Laboratory, 1999.

(28) Klippenstein, S. J. *J. Phys. Chem.* **1994**, *98*, 11459.

JP9006476